RSC Advances

PAPER

View Article Online
View Journal | View Issue

Cite this: *RSC Adv.*, 2023, **13**, 10650

Efficient and recyclable Nd^{3+}-doped $CoFe_2O_4$ for boosted visible light-driven photocatalytic degradation of Rhodamine B dye†

Loan T. T. Nguyen, [a] Hang T. T. Nguyen,[b] Lan T. H. Nguyen,[a] Anh T. T. Duong,[a] Hai Q. Nguyen,[a] Viet T. M. Ngo,[a] Nhuong V. Vu, [a] Duyen Thi Cam Nguyen[cd] and Thuan Van Tran *[cd]

Received 13th February 2023
Accepted 24th March 2023

DOI: 10.1039/d3ra00971h

rsc.li/rsc-advances

Rare earth metal doping spinel ferrites offer excellent electronic, magnetic, and photocatalytic properties, but they have not been well explored for environmental mitigation. Herein, we report the facile fabrication of novel $CoNd_xFe_{2-x}O_4$ ($x = 0$–0.05) photocatalysts based on Nd^{3+} incorporated into $CoFe_2O_4$ for the degradation of Rhodamine B under visible light irradiation. The Nd^{3+} dopant considerably increased the specific surface area (35 $m^2\ g^{-1}$) and enhanced the degradation performance (94.7%) of $CoNd_xFe_{2-x}O_4$ catalysts. Nd^{3+}-doped $CoFe_2O_4$ played a role in the formation of radicals, including $^{\bullet}OH$, h^+, and $^{\bullet}O_2^-$. With high recyclability and performance, $CoNd_{0.05}Fe_{1.95}O_4$ nanoparticles can be efficient and reusable photocatalysts for degrading organic dyes, including Rhodamine B from wastewaters.

1. Introduction

Discharging the effluent containing organic dyes into water sources has been recently posing enormous impacts on aquatic ecosystems.[1] The nature of dyes is water-soluble and low biodegradable, accumulating in durable wastewaters.[2] Consequently, they increase chemical and biochemical oxygen demands, which depletes water-dissolved oxygen, thereby causing the biological disruption of the photosynthetic activities of aquatic microorganisms.[3] The conventional methods of wastewater management, such as membrane filtration and coagulation processes, are mismatched with cost-effectiveness and performance.[4] Therefore, an increasing demand for the development of effective treatment techniques has been addressed. The visible light-driven photocatalytic dye degradation process is proposed as a feasible method with the main advantages of treatment efficiency and technical simplicity.[5]

Over the past years, nanostructured photocatalysts, including but not limited to TiO_2, ZnO, and WO_3, have observed significant growth and have been utilized for various applications in wastewater treatment, electrochemical, energy storage, and sensing.[6,7] Ferrite-based semiconductor photocatalysts are of great interest owing to their unique electronic structure and magnetism.[8] Among common ferrites, $CoFe_2O_4$ has a narrow band gap energy of 1.6–2.4 eV, making it capable of harvesting photons from visible light.[9] Despite such potential, $CoFe_2O_4$ nanoparticles still show limited photocatalytic activity because rapid recombination between electrons and holes can significantly lower the catalytic performance of $CoFe_2O_4$.[10] To address this issue, researchers have explored the use of $CoFe_2O_4$ with various rare earth dopants, such as Dy and Ce, to intercept this recombination and improve photocatalytic efficiency. Chen *et al.* reported the partial substitution of Fe^{3+} with Dy^{3+} to create a new lattice of $CoFe_2O_4$.[11] These authors observed that Dy^{3+}-doped $CoFe_2O_4$ exhibited good photocatalytic performance against methyl orange (78.7%). Zhu *et al.* synthesized Ce^{3+}-doped $CoFe_2O_4$ using the hydrothermal method and found an orange II degradation percentage of 98.5% for 60 min.[12] However, only few studies have investigated the introduction of rare earth metals into $CoFe_2O_4$ and their application in the photocatalytic removal of dyes.

Herein, we incorporated neodymium (Nd) into $CoFe_2O_4$ to enhance the photocatalytic efficiency of $CoNd_xFe_{2-x}O_4$. Nd with an electronic configure ($[Xe]4f^46s^2$) is one of the most reactive lanthanides. It is hypothesized that Nd^{3+} substitution into the lattice of $CoFe_2O_4$ leads possibly to the formation of oxygen vacancies and surface defects, enhancing the electron transfer and hindering the recombination capability of electrons and holes.[13] Although the synthesis and magnetic properties of $CoNd_xFe_{2-x}O_4$ have been reported previously, the photocatalytic performance of this nanomaterial has not yet been investigated.

[a]*Faculty of Chemistry, Thai Nguyen University of Education, Thai Nguyen 240000, Vietnam*

[b]*Faculty of Automotive and Power Machinery Engineering, Thai Nguyen University of Technology, Thai Nguyen, 24000, Vietnam*

[c]*Institute of Applied Technology and Sustainable Development, Nguyen Tat Thanh University, 298-300A Nguyen Tat Thanh, District 4, Ho Chi Minh City, 755414, Vietnam. E-mail: tranvt@ntt.edu.vn; ttran@gradcenter.cuny.edu; tranuv@gmail.com; Fax: (+84)-028-39-404-759; Tel: (+84)-028-3941-1211*

[d]*Faculty of Environmental and Food Engineering, Nguyen Tat Thanh University, 298-300A Nguyen Tat Thanh, District 4, Ho Chi Minh City 755414, Vietnam*

† Electronic supplementary information (ESI) available. See DOI: https://doi.org/10.1039/d3ra00971h

Therefore, this study aims to synthesize and investigate photocatalytic $CoNd_xFe_{2-x}O_4$ with different Nd^{3+} doping ratios from 0 to 5% by molar. The structure of the $CoNd_xFe_{2-x}O_4$ nanocomposites was analyzed, and their photocatalytic activity was examined under visible light. In addition, the plausible mechanism of Rhodamine B degradation in the presence of $CoNd_xFe_{2-x}O_4/H_2O_2$/visible light catalytic system was suggested.

2. Experimental

2.1. Synthesis of Nd-doped $CoFe_2O_4$ nanocomposites

Nd^{3+}-doped $CoFe_2O_4$, other names $CoNd_xFe_{2-x}O_4$ ($x = 0$, 0.01, 0.03, 0.05), could be facilely synthesized as follows. The process involved dissolving 500 mg of urea, 1 mmol of cobalt nitrate, $(2-x)$ mmol of iron(III) nitrate and x mmol of neodymium nitrate in 30 mL of pure H_2O. The liquid was heated to 100 °C under stirring, maintained at this temperature for 6 h, and dried in an oven overnight. The solid was calcined at 500 °C for 4 h to obtain the final $CoNd_xFe_{2-x}O_4$ products.

2.2. Photocatalytic experiments

To assess the efficiency of Nd^{3+}-doped $CoFe_2O_4$ nanocomposites in photodegradation reaction, a visible-light source of 30 W provided by LED lamp emitting light within the wavelength range of 400–700 nm filtered by a UV filter, with a rate luminous flux of 2300 lm, and a color rendering index of 80 was used. The light source was fixed 12 cm higher than the RhB solution surface. To begin the experiment, a fixed amount (0.75 g L^{-1}) of the $CoNd_xFe_{2-x}O_4$ was added to 0.1 L of 10 mg L^{-1} Rhodamine B solution. Subsequently, a 30% hydroperoxide solution was slowly dropwised to reach a concentration of 0.1 M. After sorption in the dark was equilibrated for 60 min, the photocatalytic system was exposed to a visible light source for 0–180 min. The concentration of RhB was calibrated using a UV-Vis spectrophotometer at 554 nm. The effect of $CoNd_xFe_{2-x}O_4$ dose on RhB degradation efficiency was examined at 0.5, 0.75, and 1 g L^{-1}, while H_2O_2 concentration was tested at 0.05, 0.1, and 0.15 M.

2.3. Recyclability study

After the catalytic experiment was completed, the $CoNd_{0.05}Fe_{1.95}O_4$ catalyst was separated from the reaction and washed with pure water and ethanol to clean the Rhodamine B dye. Afterward, the reused $CoNd_{0.05}Fe_{1.95}O_4$ was dried overnight in an oven and used as a catalyst for further experiments. In detail, 0.75 g L^{-1} of recycled $CoNd_xFe_{2-x}O_4$ and 30% H_2O_2 with a concentration of 0.1 M were added to 0.1 L of 10 mg L^{-1} Rhodamine B solution. After 60 min of stirring in the dark, the photocatalytic system was exposed to a visible light source for 180 min. This process was repeated until the degradation efficiency against Rhodamine B dye was significantly reduced.

3. Results and discussion

3.1. Characterization

The X-ray diffraction patterns of $CoNd_xFe_{2-x}O_4$ ($x = 0$, 0.01, 0.03, 0.05) nanoparticles are characterized, as shown in Fig. 1a. Diffraction patterns indicated the presence of well-defined peaks at 2θ degrees for the as-synthesized $CoFe_2O_4$, with lattice planes at 30.2° (220), 35.3° (331), 43.2° (400), 54.8° (422), 57.1° (511), and 62.7° (440) matching the standard pattern of spinel cubic $CoFe_2O_4$ structure as per JCPDS card no. 03-0864. The presence of ortho-ferrite $NdFeO_3$ single phase became more prominent with increased Nd^{3+} dopants caused by the substitution of Fe^{3+} by Nd^{3+}. Because Nd^{3+} ions have a larger radius than those of Fe^{3+}, the atomic substitution in the $CoFe_2O_4$ lattice is restrained, resulting in the aggregation of Nd^{3+} on the grain boundary to form $NdFeO_3$.[14] As Fe^{3+} substituted by Nd^{3+} increased, the peak intensity at the (311) plane increased, and a slight shift in the (311) angle as a result of unstable d-spacing was observed in Table S1,† confirming the transfer of Nd^{3+} ions into octahedral and tetrahedral sites to replace Co^{2+}/Fe^{3+} ions. $CoNd_xFe_{2-x}O_4$ crystallite sizes were calculated based on the Scherrer equation for full width at half maximum of the (311) plane. Table S1† shows an upward crystallite size trend (14.35–29.14 nm) with increasing Nd^{3+} dopant, which suggests that Nd^{3+} substitution might extend unit cells, leading to increased lattice constants.

The surface chemistry of Nd-doped $CoFe_2O_4$ can be examined using the FT-IR spectra, as illustrated in Fig. 1b. The two transmittance bands ν_1 and ν_2 shown in Table S1† reflect tetrahedral and octahedral metal (Fe, Nd)-oxygen bonds, respectively. Absorption bands shifting increasingly to the high-frequency band were attributable to altering lattice parameters and ionic redistribution as a result of the incorporation of rare earth-like Nd^{3+} into the spinel $CoFe_2O_4$ structure.[15] The optical characteristics and Tauc plots of $(\alpha h\nu)^2$ *versus* photon energy ($h\nu$) of $CoNd_xFe_{2-x}O_4$ can be evaluated using UV-Vis DRS spectra, as depicted in Fig. S1.† It is noticeable that the bandgap energy (E_g) decreased (1.57–1.35 eV) as the Nd^{3+} doping (0–5%) increased, confirming the change in the electric structure of $CoNd_xFe_{2-x}O_4$ a result of the bandgap renormalization effect.[16] Specifically, a dynamic screening of Coulomb repulsion may decrease the electronic bandgap of the $CoNd_xFe_{2-x}O_4$ semiconductor as it partially cancels the Moss–Burstein shift.[17] The result contradicted an enhanced bandgap caused by the quantum confinement effect as reported previously.[18] Moreover, magnetic properties of $CoNd_xFe_{2-x}O_4$ *via* vibrating sample magnetometer showed that magnetic hysteresis loops were smaller and saturation magnetization values decreased from 47 to 29 emu g^{-1} with higher Nd^{3+} doping in $CoFe_2O_4$ (Fig. S2†). The magnetic results herein agree with the previous report,[19] which can be normally due to the lower paramagnetic moment of substituted Nd^{3+} ions than ferromagnetic Fe^{3+} ions.

Fig. 1c shows N_2 adsorption/desorption isotherm plots of $CoFe_2O_4$ and $CoNd_{0.05}Fe_{1.95}O_4$ with the characteristics of Type II (nonporous or macroporous) based on IUPAC classification. $CoFe_2O_4$. However, a minor hysteresis loop (H_2) of $CoNd_{0.05}Fe_{1.95}O_4$ rather than $CoFe_2O_4$ was observed, indicating a disordered, well-undefined and defected interface of $CoNd_{0.05}Fe_{1.95}O_4$.[20] Incorporating Nd^{3+} ions into $CoFe_2O_4$ lattice caused the redistribution of Co^{2+}/Fe^{3+} cations and defected crystal lattice.[21] The specific surface area of $CoNd_{0.05}Fe_{1.95}O_4$ was 35.0 m^2 g^{-1} compared with 12.7 m^2 g^{-1} for $CoFe_2O_4$ (Table

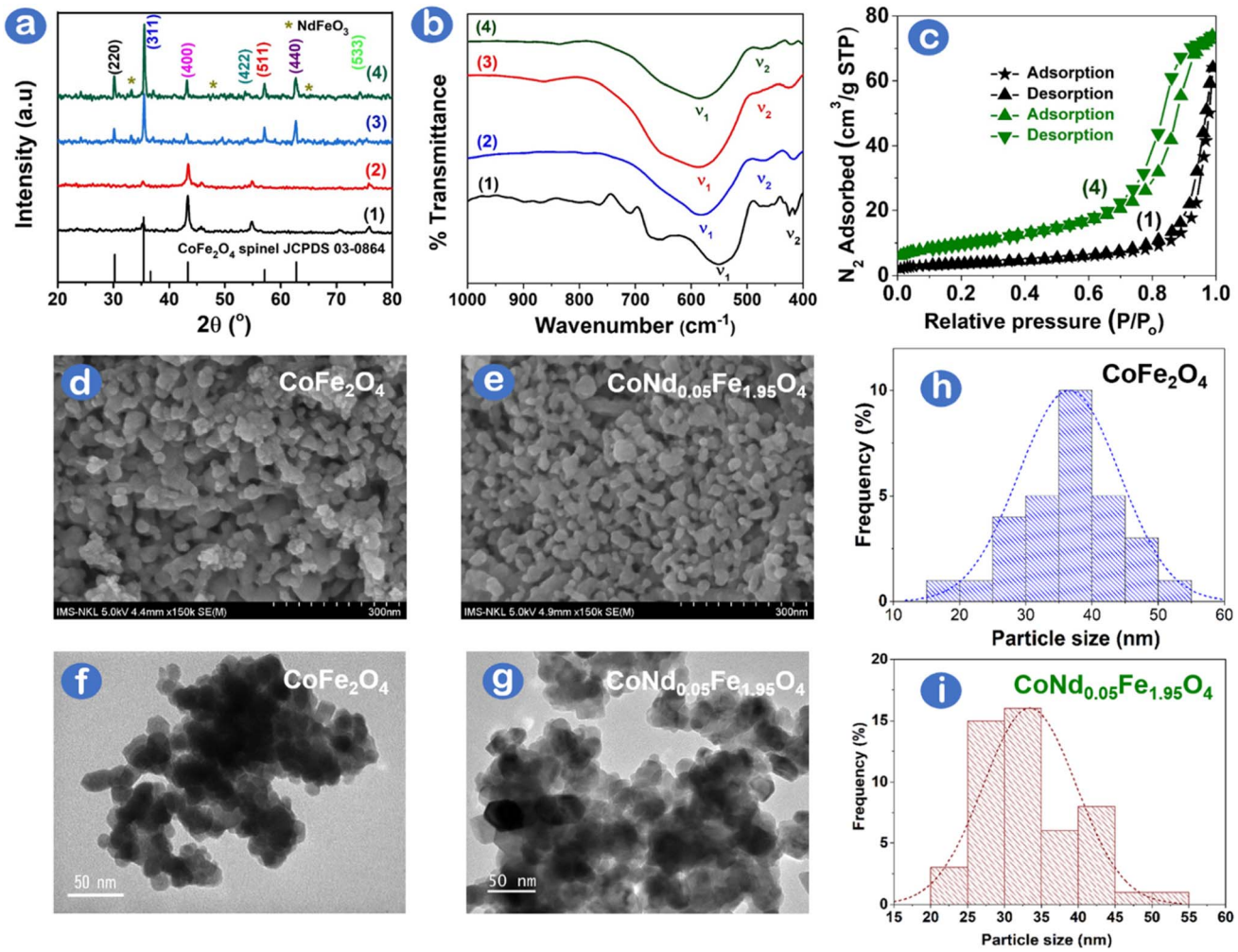

Fig. 1 (a) XRD patterns, (b) FTIR spectra, (c) N_2 adsorption–desorption isotherm curves, (d, e) SEM images, (f, g) TEM images, and (h, i) particle size distribution histograms of (1) $CoFe_2O_4$, (2) $CoNd_{0.01}Fe_{1.99}O_4$, (3) $CoNd_{0.03}Fe_{1.97}O_4$ and (4) $CoNd_{0.05}Fe_{1.95}O_4$ catalysts.

S2†). The total pore volume of $CoNd_{0.05}Fe_{1.95}O_4$ (0.114 $cm^3\ g^{-1}$) was also higher than that of $CoFe_2O_4$ (0.099 $cm^3\ g^{-1}$), suggesting that Nd^{3+} substitution improved the porosity of the origin spinel ferrite. It was interpreted that doping of neodymium elements might optimize the surface structure of cobalt ferrite, leading to a decrease in grain size with an enhanced porous structure and surface area. The substitution of other rare earth metals (*e.g.*, Ce^{3+}, La^{3+}, and Y^{3+}) into $CoFe_2O_4$ was also found to significantly increase the surface area (4.39–6.95 $m^2\ g^{-1}$) of rare earth-modified $CoFe_2O_4$ compared with bare $CoFe_2O_4$ (2.13 $m^2\ g^{-1}$) as reported by Gao *et al.*[22] With higher area and defected surface, $CoNd_{0.05}Fe_{1.95}O_4$ was expected to have more active sites for photocatalytic performance.

The morphology and inherent structure of $CoFe_2O_4$ and $CoNd_{0.05}Fe_{1.95}O_4$ are examined by SEM/TEM images, as illustrated in Fig. 1d–g. $CoFe_2O_4$ and $CoNd_{0.05}Fe_{1.95}O_4$ exhibit nanospherical nanoparticles, with a slight degree of clustering, which was highly commensurate with the morphology of Nd^{3+} doped $CoFe_2O_4$ as published previously.[21,23] A minor decrease in average particle size from 35 nm ($CoFe_2O_4$) to 30 nm ($CoNd_{0.05}Fe_{1.95}O_4$) is shown in Fig. 1h and g. This trend can be explained that Nd^{3+} incorporation might intercept the crystal growth of $CoFe_2O_4$ during combustion synthesis. Fig. S3† illustrates the chemical composition of nanocomposites with three major elements (11.44% Co, 26.94% Fe, and 61.62% O) for $CoFe_2O_4$ and four major elements (13.41% Co, 21.34% Fe, 64.59% O, and 0.66% Nd) for $CoNd_{0.05}Fe_{1.95}O_4$. Otherwise, no unusual peaks in the EDX spectra suggest that the samples are highly pure.

3.2. Photocatalytic study

The catalytic photodegradation of Rhodamine B dye as a test substance in the presence of $CoNd_xFe_{2-x}O_4$ (x = 0, 0.01, 0.03, and 0.05) nanoparticles was conducted, as depicted in Fig. 2a. As depicted in Table S3,† the Rhodamine B removal percentage was almost insufficient (12.9–29.4%) in the absence of either the $CoFe_2O_4$ catalyst or H_2O_2 oxidant under visible light. The reaction rates were also slow (0.7×10^{-3}–1.4×10^{-3} min^{-1}) in these cases, indicating that Rhodamine B dye could be removed owing to adsorption onto $CoFe_2O_4$. When both 0.1 M H_2O_2 and

$CoFe_2O_4$ catalysts were added under visible light conditions, 71.7% of Rhodamine B dye was removed by $CoFe_2O_4$. It is therefore believed that the catalyst, oxidant, and visible light source played a necessary role in the photocatalytic degradation of Rhodamine B dye. With increasing ratios of Nd^{3+} doping (0–0.05), the catalysts exhibited improved catalytic activity for the degradation of Rhodamine B dye (68.2–94.7%). The highest degradation efficiency and kinetic rate were observed under a $CoNd_{0.05}Fe_{1.95}O_4/H_2O_2$/visible light system at 94.7% for 180 min and 5.3×10^{-3} min^{-1}, respectively. With a higher doping of Nd^{3+} ($x = 0.01$), however, the $CoNd_{0.1}Fe_{1.9}O_4$ showed lower catalytic activity, with 85.1% of RhB degradation efficiency. This finding could, therefore, be because of the contribution of 5% Nd^{3+} substituted in $CoFe_2O_4$ lattice that is enough for accelerating electron transfer and prevention of electron–hole recombination.

To assess the amount of oxygen necessary to oxidize the organic matter in aquatic wastewaters, the chemical oxygen demand (COD) index was measured. The results of the photocatalytic study of $CoNd_xFe_{2-x}O_4$ nanocomposites on the removal of Rhodamine B dye are shown in Fig. 2b. The COD percentage obtained after 360 min is as follows: $CoFe_2O_4$ (71.7%) < $CoNd_{0.01}Fe_{1.99}O_4$ (76.5%) < $CoNd_{0.03}Fe_{1.97}O_4$ (81.2%) < $CoNd_{0.05}Fe_{1.95}O_4$ (89.5%). The best catalyst, $CoNd_{0.05}Fe_{1.95}O_4$, was able to significantly reduce the COD value of the Rhodamine B wastewater sample from 394.7 mg L^{-1} to 41.0 mg L^{-1}. This result demonstrates an efficient Rhodamine B mineralization of $CoNd_{0.05}Fe_{1.95}O_4$ into less toxic compounds, such as CO_2, H_2O, and N_2.[24,25] Several photocatalytic degradation pathways for the mineralization of Rhodamine B could be deethylation, ring opening, and degradation of aryl chromophore.[26] Overall, our results indicated a good degree of RhB dye mineralization catalyzed by $CoNd_{0.05}Fe_{1.95}O_4$, which can make dyes-containing wastewater cleaner and safer.

Several factors (*e.g.*, catalyst loading and H_2O_2 concentration) can influence the visible light photocatalytic degradation reaction of Rhodamine B. Fig. 2c shows that the optimal amount of $CoNd_{0.05}Fe_{1.95}O_4$ catalyst was 0.75 g L^{-1}, which led to a 93.4% removal efficiency of the Rhodamine B dye. Furthermore, the influence of H_2O_2 concentration was studied, with oxidant concentrations ranging from 0.05 to 0.15 M. Fig. 2d depicts that 0.1 M H_2O_2 concentration was found to be optimal, as this oxidant provided a sufficient amount of reactive oxygen radicals for the degradation of dyes.

Scavenging experiments can be performed to comprehend the significance of radicals, such as $^{\bullet}OH$ and $^{\bullet}O_2^-$, under $CoNd_{0.05}Fe_{1.95}O_4/H_2O_2$/visible-light system. Fig. 3a illustrates that the Rhodamine B degradation efficiencies of Rhodamine B dye over $CoNd_{0.05}Fe_{1.95}O_4$ catalyst were considerably reduced (49.8–61.6%) as one of the scavengers for trapping radicals, *e.g.*, ascorbic acid ($^{\bullet}O_2^-$), ethylenediaminetetraacetic acid (h^+), and isopropyl alcohol ($^{\bullet}OH$), was added into the reaction. Table S4† shows a comparison of degradation efficiencies and pseudo-first order kinetic rates (k_1) as follows: EDTA (49.8%, 2.7 ×

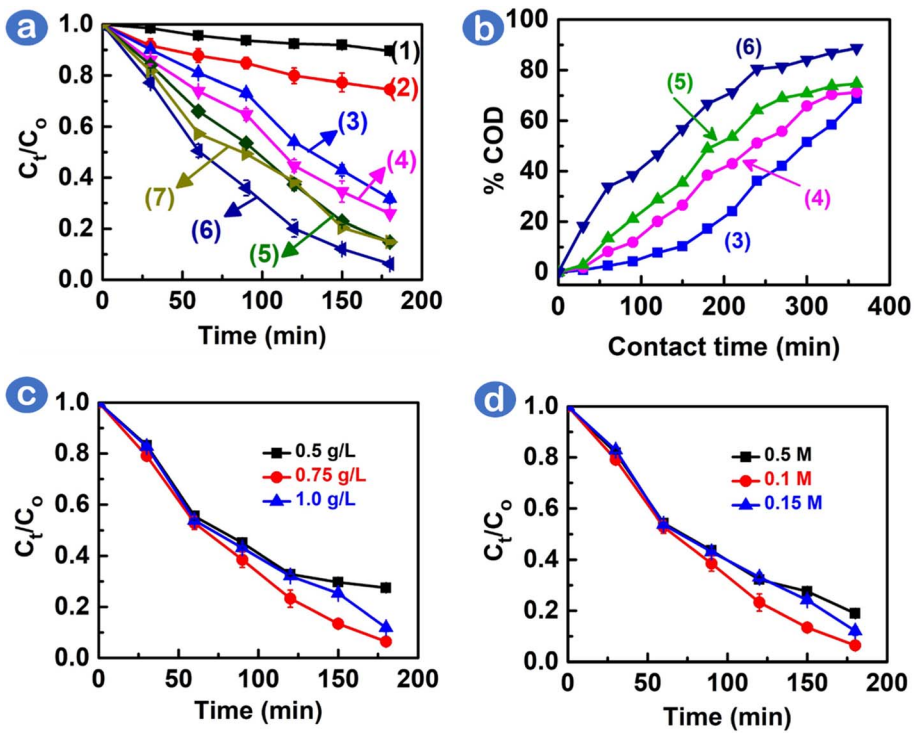

Fig. 2 (a) Rhodamine B degradation in the presence of (1) H_2O_2 only, (2) $CoFe_2O_4$ catalyst only, (3) H_2O_2 + $CoFe_2O_4$, (4) H_2O_2 + $CoNd_{0.01}Fe_{1.99}O_4$, (5) H_2O_2 + $CoNd_{0.03}Fe_{1.97}O_4$, (6) H_2O_2 + $CoNd_{0.05}Fe_{1.95}O_4$, and (7) H_2O_2 + $CoNd_{0.1}Fe_{1.9}O_4$; (b) comparative reduction efficiencies of chemical oxygen demand index among various catalysts; (c) impact of $CoNd_{0.05}Fe_{1.95}O_4$ loadings (0.5, 0.75, and 1 g L^{-1}); (d) impact of H_2O_2 concentrations (0.05, 0.1, and 0.15 M).

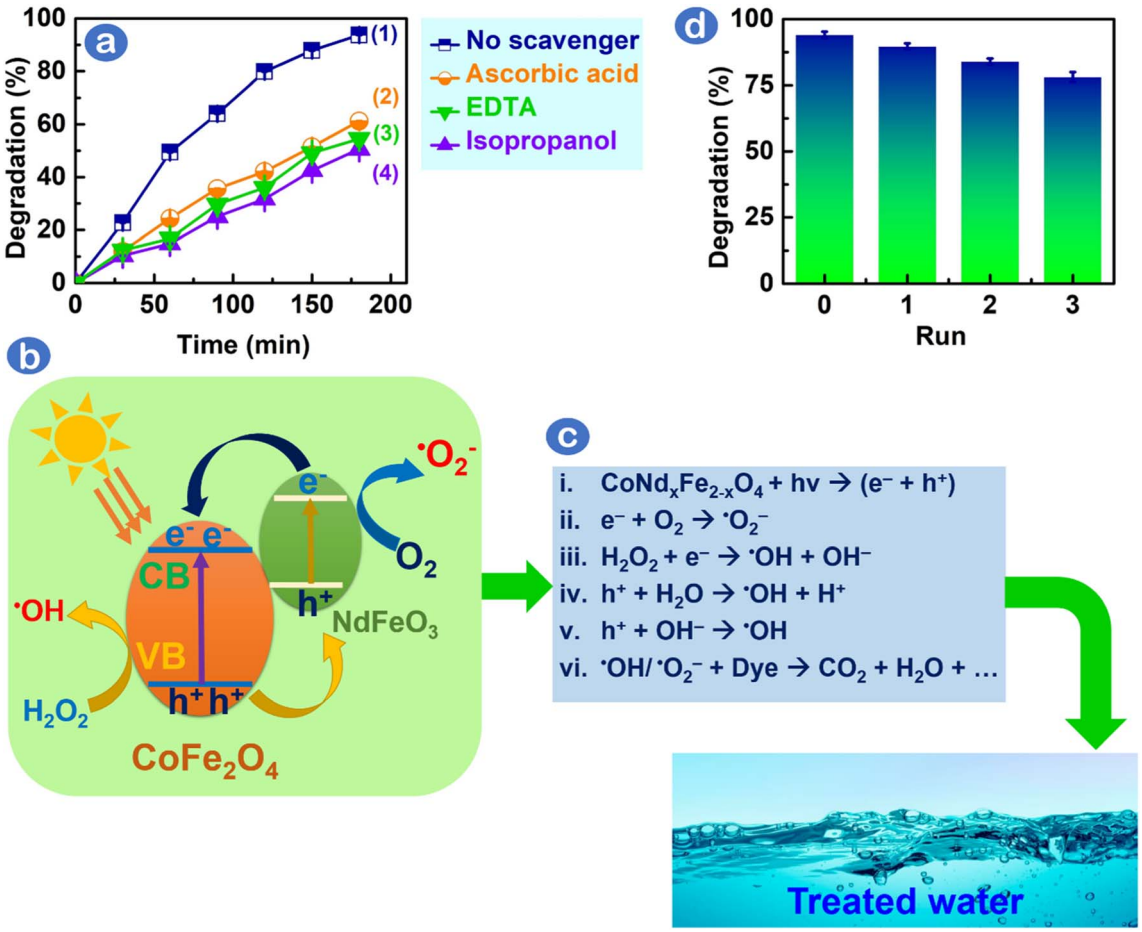

Fig. 3 (a) Rhodamine B removal efficiencies under $CoNd_{0.05}Fe_{1.95}O_4/H_2O_2$/visible light photocatalytic system, (1) no scavenger was added, (2) ascorbic acid was added, (3) ethylenediaminetetraacetic acid was added, and (4) isopropyl alcohol was added (4); (b and c) plausible Rhodamine B degradation mechanisms using $CoNd_{0.05}Fe_{1.95}O_4/H_2O_2$/visible-light system; and (d) recyclability study for $CoNd_{0.05}Fe_{1.95}O_4$ catalyst.

10^{-3} min^{-1}) < isopropyl alcohol (52.1%, 2.9 × 10^{-3} min^{-1}) < ascorbic acid (61.6%, 3.4 × 10^{-3} min^{-1}) < no scavengers (93.7%, 5.3 × 10^{-3} min^{-1}). Because the degradation efficiency did not differ significantly under various scavengers, radical species, including $^{\bullet}OH$, $^{\bullet}O_2^-$, and h^+, might take main responsibility for the degradation of Rhodamine B.

The role of radicals ($^{\bullet}OH$, $^{\bullet}O_2^-$, and h^+) on Rhodamine B degradation catalyzed by $CoNd_{0.05}Fe_{1.95}O_4$ under visible light is elucidated herein, as demonstrated in Fig. 3b. Initially, incorporating Nd^{3+} into $CoFe_2O_4$ changes the electronic density and metal–oxygen bonding energy in $CoFe_2O_4$ crystal lattice, thereby exerting the formation of oxygen vacancies and defected surface on $CoNd_{0.05}Fe_{1.95}O_4$ photocatalyst.[23] Partially filled f-orbitals of Nd^{3+} ions (Nd^{3+}/Nd^{2+}, $E^0 = -0.40$ V *vs.* NHE) enable visible light-photoexcited electrons to transfer easily from the valence band of $CoFe_2O_4$ to the Nd^{3+} doping energy level in $NdFeO_3$.[27] Consequently, Nd^{3+} f-orbitals might hinder the photogenerated e^-/h^+ pair recombination, thereby improving degradation performance. Fig. 3c illustrates the interaction between e^- and O_2 to create $^{\bullet}O_2^-$ and between e^- and H_2O_2 to create $^{\bullet}OH$. Holes (h^+) interact with H_2O/OH^- to form $^{\bullet}OH$. It is suggested that $^{\bullet}OH$ and $^{\bullet}O_2^-$ species reacted with Rhodamine B to degrade into mediators, fragments and final products, such as H_2O and CO_2. To assess the stability of $CoNd_{0.05}Fe_{1.95}O_4$, we examined Rhodamine B degradation efficiency after the photocatalytic cycle. As shown in Fig. 3d, $CoNd_{0.05}Fe_{1.95}O_4$ can be reused several times, and the final cycle showed a degradation efficiency of 78%, suggesting that this catalyst had high stability. To check the crystalline structure of the $CoNd_{0.05}Fe_{1.95}O_4$ catalyst after use, XRD patterns were examined, as depicted in Fig. S4.† The primary peaks at (220), (311), (400), (422), (511), (440), and (533) were still maintained, suggesting that the $CoNd_{0.05}Fe_{1.95}O_4$ structure was stable after the recycling process.

The photocatalytic efficiency of $CoNd_{0.05}Fe_{1.95}O_4$ can be compared with other catalysts. As depicted in Table 1, $CoNd_{0.05}Fe_{1.95}O_4$ in this study demonstrated higher dye degradation performance (94.7%) than other photocatalysts. Moreover, this reaction was conducted under mild conditions, *i.e.*, a visible light source instead of a UV light condition, as reported in previous studies. This comparison suggests that the $CoNd_{0.05}Fe_{1.95}O_4$ could be a competitive photocatalyst for degrading hazardous dyes, such as Rhodamine B, in wastewater under visible light condition.

Table 1 Comparative data on the Rhodamine B degradation efficiency of various photocatalysts

No.	Nanocomposite	Light source	H (%)	Ref.
1	$CoNd_{0.05}Fe_{1.95}O_4$	Visible light	94.7	This work
2	$ZnFe_2O_4$-50%@ZnO	Visible light	79	28
3	$NiFe_2O_4$@HAp-Sn^{2+}	Visible light	84.4	29
4	$NiFe_2O_4$	Visible light	90	30
5	ZnFe@CuS	Visible light	93	31
6	$ZnFe_2O_4$	Visible light	94	30
7	MIL-101(Cr)/RGO/$ZnFe_2O_4$	Visible light	94	24
8	$ZnFe_2O_4$/graphene oxide	Visible light	94	32
9	$Ni_{0.5}Zn_{0.5}Fe_2O_4$	Visible light	98	30
10	Zn-doped Fe_3O_4	UV light	97	33
11	$NiFe_2O_4$	UV light	84	34
12	AuSe QDs@$Cs_2Fe_2O_4$	UV light	99.2	35
13	$Mg_{0.4}Zn_{(0.6-xx)}Ca_xFe_2O_4$	UV light	99.5	36
14	Chitin biochar-based $ZnFe_2O_4$	Solar light	100	37

4. Conclusion

Novel $CoNd_xFe_{2-x}O_4$ catalysts with various amounts of Nd^{3+} dopant were synthesized and characterized. Nd^{3+} substitution into $CoFe_2O_4$ lattice changed its electronic and magnetic structure. Bandgaps and saturation magnetization decreased as the Nd^{3+} doping increased. Moreover, $CoNd_{0.05}Fe_{1.95}O_4$ obtained small particle sizes and a large surface area (35 $m^2\ g^{-1}$). The highest degradation efficiency was obtained (94.7%) at 0.75 g L^{-1} of $CoNd_{0.05}Fe_{1.95}O_4$ and 0.1 M H_2O_2 under visible light irradiation. The main radical species, such as $^{\bullet}OH$, h^+, and $^{\bullet}O_2^-$, were found to influence the mechanism of Rhodamine B dye degradation. Additionally, the catalyst demonstrated good stability and recyclability. These results suggest that $CoNd_{0.05}Fe_{1.95}O_4$ nanoparticles can be an efficient and reusable photocatalyst for degrading organic dyes in water.

Conflicts of interest

There are no conflicts of interest to declare.

Acknowledgements

This research is funded by Thai Nguyen University of Education under grant number TNUE-2022-05.

References

1 R. Al-Tohamy, S. S. Ali, F. Li, K. M. Okasha, Y. A. G. Mahmoud, T. Elsamahy, H. Jiao, Y. Fu and J. Sun, *Ecotoxicol. Environ. Saf.*, 2022, **231**, 113160.
2 T. V. Tran, D. T. C. Nguyen, P. S. Kumar, A. T. M. Din, A. S. Qazaq and D.-V. N. Vo, *Environ. Res.*, 2022, **214**, 113925.
3 M. Shabir, M. Yasin, M. Hussain, I. Shafiq, P. Akhter, A.-S. Nizami, B.-H. Jeon and Y.-K. Park, *J. Ind. Eng. Chem.*, 2022, **112**, 1–19.
4 R. Yadav, T. S. Chundawat, P. K. Surolia and D. Vaya, *J. Phys. Chem. Solids*, 2022, **165**, 110691.
5 T. Wang, J. Zheng, J. Cai, Q. Liu and X. Zhang, *Sci. Total Environ.*, 2022, **839**, 155955.
6 J. Lincho, A. Zaleska-Medynska, R. C. Martins and J. Gomes, *Sci. Total Environ.*, 2022, **837**, 155776.
7 F. Siddique, S. Gonzalez-Cortes, A. Mirzaei, T. Xiao, M. A. Rafiq and X. Zhang, *Nanoscale*, 2022, **14**, 11806–11868.
8 H. S. Jarusheh, A. Yusuf, F. Banat, M. A. Haija and G. Palmisano, *J. Environ. Chem. Eng.*, 2022, **10**, 108204.
9 J. Chen, Y. Wang and Y. Deng, *J. Alloys Compd.*, 2013, **552**, 65–69.
10 B. Aslibeiki, N. Eskandarzadeh, H. Jalili, A. Ghotbi Varzaneh, P. Kameli, I. Orue, V. Chernenko, A. Hajalilou, L. P. Ferreira and M. M. Cruz, *Ceram. Int.*, 2022, **48**, 27995–28005.
11 S. Chen, D. Jiang, G. Zeng, H. Chi, L. Li, Y. He, F. Ke, J. D. Xiao and S. Ye, *Mater. Lett.*, 2021, **284**, 128966.
12 F. Zhu, Q. Ji, Y. Lei, J. Ma, Q. Xiao, Y. Yang and S. Komarneni, *Chemosphere*, 2022, **291**, 132765.
13 F. Sharifianjazi, M. Moradi, N. Parvin, A. Nemati, A. Jafari Rad, N. Sheysi, A. Abouchenari, A. Mohammadi, S. Karbasi, Z. Ahmadi, A. Esmaeilkhanian, M. Irani, A. Pakseresht, S. Sahmani and M. Shahedi Asl, *Ceram. Int.*, 2020, **46**, 18391–18412.
14 R. S. Yadav, J. Havlica, J. Masilko, L. Kalina, J. Wasserbauer, M. Hajdúchová, V. Enev, I. Kuřitka and Z. Kožáková, *J. Magn. Magn. Mater.*, 2016, **399**, 109–117.
15 Z. A. Gilani, M. F. Warsi, M. N. Anjum, I. Shakir, S. Naseem, S. Riaz and M. A. Khan, *J. Alloys Compd.*, 2015, **639**, 268–273.
16 M. M. Ugeda, A. J. Bradley, S.-F. Shi, F. H. da Jornada, Y. Zhang, D. Y. Qiu, W. Ruan, S.-K. Mo, Z. Hussain, Z.-X. Shen, F. Wang, S. G. Louie and M. F. Crommie, *Nat. Mater.*, 2014, **13**, 1091–1095.
17 P. D. Cunningham, A. T. Hanbicki, K. M. McCreary and B. T. Jonker, *ACS Nano*, 2017, **11**, 12601–12608.
18 A. M. S. Arulanantham, K. V. Gunavathy, M. Antony, N. Sundaramurthy, M. M. Stephy, P. Mohanraj and V. Ganesh, *Chem. Pap.*, 2022, **76**, 6349–6358.
19 M. A. Ahmed, N. Okasha, A. A. Mohamed and I. Mmdouh, *J. Magn. Magn. Mater.*, 2014, **358–359**, 32–37.
20 A. Svidrytski, D. Hlushkou, M. Thommes, P. A. Monson and U. Tallarek, *J. Phys. Chem. C*, 2020, **124**, 21646–21655.
21 M. A. Almessiere, Y. Slimani, S. Güner, M. Nawaz, A. Baykal, F. Aldakheel, S. Akhtar, I. Ercan, I. Belenli and B. Ozçelik, *Ceram. Int.*, 2019, **45**, 8222–8232.
22 J. Gao, G. Pu, C. Yuan, M. Gao, X. Lu and S. Jia, *Fuel*, 2022, **326**, 124933.
23 K. L. Routray, S. Saha, D. Sanyal and D. Behera, *Mater. Res. Express*, 2019, **6**, 026107.
24 L. Nirumand, S. Farhadi, A. Zabardasti and A. Khataee, *Ultrason. Sonochem.*, 2018, **42**, 647–658.
25 A. H. Mady, M. L. Baynosa, D. Tuma and J. J. Shim, *Appl. Catal., B*, 2017, **203**, 416–427.
26 L. T. T. Nguyen, H. T. T. Nguyen, L. T. H. Nguyen, A. T. T. Duong, H. Q. Nguyen, N. D. Bui, V. T. M. Ngo, D. T. C. Nguyen and T. V. Tran, *Environ. Res.*, 2022, **214**, 114130.
27 G. L. Colpani, R. C. F. Zeferino, M. Zanetti, J. M. M. Mello, L. L. Silva and M. A. Fiori, in *Photocatalytic Systems by*

Design: Materials, Mechanisms and Applications, Elsevier, 2021, pp. 23–53.

28 L. T. T. Nguyen, D.-V. N. Vo, L. T. H. Nguyen, A. T. T. Duong, H. Q. Nguyen, N. M. Chu, D. T. C. Nguyen and T. V. Tran, *Environ. Technol. Innovation*, 2022, **25**, 102130.

29 K. C. Das, S. S. Dhar, D. G. Thakurata and J. Das, *J. Cleaner Prod.*, 2021, **290**, 125172.

30 S. A. Jadhav, M. V. Khedkar, D. D. Andhare, S. B. Gopale and K. M. Jadhav, *Ceram. Int.*, 2021, **47**, 13980–13993.

31 M. Shakil, U. Inayat, M. Ashraf, M. Tanveer, S. S. A. Gillani and A. Dahshan, *Optik*, 2023, **272**, 170353.

32 N. Nadeem, M. Zahid, A. Tabasum, A. Mansha, A. Jilani, I. A. Bhatti and H. N. Bhatti, *Mater. Res. Express*, 2020, **7**, 15519.

33 A. Manohar, K. Chintagumpala and K. H. Kim, *J. Mater. Sci.: Mater. Electron.*, 2021, **32**, 8778–8787.

34 K. R. Sanadi, K. C. Rathod, M. L. Gaur, R. R. Powar, V. G. Parale, R. S. Patil, S. H. Burungale and A. V. Mali, *Bull. Mater. Sci.*, 2021, **44**, 265.

35 F. T. Alshorifi, A. A. Alswat and R. S. Salama, *Heliyon*, 2022, **8**, e09652.

36 S. Kumari, N. Dhanda, A. Thakur, V. Gupta, S. Singh, R. Kumar, S. Hameed and P. Thakur, *Ceram. Int.*, 2023, **49**(8), 12469–12480.

37 N. Welter, J. Leichtweis, S. Silvestri, P. I. Z. Sánchez, A. C. C. Mejía and E. Carissimi, *J. Alloys Compd.*, 2022, **901**, 163758.